Nanoscale Res Lett (2010) 5:169–173
DOI 10.1007/s11671-009-9460-1

NANO EXPRESS

Snap-Through Instability of Graphene on Substrates

Teng Li · Zhao Zhang

Received: 6 August 2009 / Accepted: 2 October 2009 / Published online: 17 October 2009
© to the authors 2009

Abstract We determine the graphene morphology regulated by substrates with herringbone and checkerboard surface corrugations. As the graphene–substrate interfacial bonding energy and the substrate surface roughness vary, the graphene morphology snaps between two distinct states: (1) closely conforming to the substrate and (2) remaining nearly flat on the substrate. Since the graphene morphology is strongly tied to the electronic properties of graphene, such a snap-through instability of graphene morphology can lead to desirable graphene electronic properties that could potentially enable graphene-based functional electronic components (e.g. nano-switches).

Keywords Graphene · Nanopatterns · Morphology · Instability · Substrate regulation

Introduction

Graphene is a monolayer of carbon atoms densely packed in a honeycomb crystal lattice. It exhibits extraordinary electrical and mechanical properties [1–5], and has inspired an array of tantalizing potential applications (e.g., transparent flexible displays and biochemical sensor arrays) [6–10]. Graphene is intrinsically non-flat and tends to be randomly corrugated [11, 12]. The random graphene morphology can lead to unstable performance of graphene devices as the corrugating physics of graphene is closely tied to its electronic properties [13, 14]. Future success of graphene-based applications hinges upon precise control of the graphene morphology over large areas, a significant challenge largely unexplored so far. Recent experiments show that, however, the morphology of graphene can be regulated by the surface of an underlying substrate [15–19]. In this paper, we quantitatively determine the regulated graphene morphology on substrates with various engineered surface patterns, using energy minimization. The results reveal the snap-through instability of graphene on substrates, a promising mechanism to enable functional components for graphene devices.

Recent experiments show that monolayer and few-layer graphene can partially follow the rough surface of the underlying substrates [15–19]. The resulting graphene morphology is regulated, rather than the intrinsic random corrugations in freestanding graphene. The substrate-regulated graphene morphology results from the interplay between the interfacial bonding energy and the strain energy of the graphene-substrate system [15, 17], which can be explained as follows.

When graphene is fabricated on a substrate surface via mechanical exfoliation [3] or transfer printing [10, 20], the graphene–substrate interfacial bonding energy is usually weak (e.g., van der Waals interaction). As the graphene corrugates to follow the substrate surface, the graphene–substrate interaction energy decreases due to the nature of van der Waals interaction; on the other hand, the strain energy in the system increases due to the intrinsic bending rigidity of graphene. At the equilibrium graphene morphology on the substrate, the sum of the interaction energy and the system strain energy reaches its minimum.

The above energetic consideration can be used to quantitatively determine the regulated graphene morphology on

T. Li (✉) · Z. Zhang
Department of Mechanical Engineering, University of Maryland, College Park, MD 20742, USA
e-mail: LiT@umd.edu

T. Li · Z. Zhang
Maryland NanoCenter, University of Maryland, College Park, MD 20742, USA

a rough substrate surface. Furthermore, with a systematic understanding of the governing mechanisms of substrate-regulated graphene morphology, we envision a promising strategy to precisely pattern graphene into desired morphology on engineered substrate surfaces. In this paper, we illustrate this strategy by determining the regulated graphene morphology on two types of engineered substrate surfaces: herringbone corrugations and checkerboard corrugations (Fig. 1). These substrate surface features can be fabricated via approaches combining lithography [21, 22] and strain engineering [23, 24].

Computational Model

The graphene–substrate interaction energy can be determined by summing up all van der Waals forces between the graphene carbon atoms and the substrate atoms. The van der Waals force between a graphene–substrate atomic pair of distance r can be characterized by a Lennard–Jones pair potential, $V_{\mathrm{LJ}}(r) = 4\varepsilon(\sigma^{12}/r^{12} - \sigma^{6}/r^{6})$, where $\sqrt[6]{2}\sigma$ is the equilibrium distance of the atomic pair and ε is the bonding energy at the equilibrium distance. The number of atoms over an area $\mathrm{d}S$ on the graphene and a volume $\mathrm{d}V_{\mathrm{s}}$ in the substrate are $\rho_{\mathrm{c}}\mathrm{d}S$ and $\rho_{\mathrm{s}}\mathrm{d}V_s$, respectively, where ρ_{c} is the homogenized carbon atom area density of graphene that is related to the equilibrium carbon–carbon bond length l by $\rho_{\mathrm{C}} = 4/(3\sqrt{3}l^2)$, and ρ_{s} is the molecular density of substrate that can be derived from the molecular mass and mass density of substrate. The interaction energy, denoted by E_{int}, between a graphene of area S and a substrate of volume V_{s} is then given by

$$E_{\mathrm{int}} = \int_S \int_{V_{\mathrm{s}}} V_{\mathrm{LJ}}(r)\rho_{\mathrm{s}}\mathrm{d}V_{\mathrm{s}}\rho_{\mathrm{c}}\mathrm{d}S. \tag{1}$$

Since Lennard–Jones potential decays rapidly beyond equilibrium atomic pair distance, E_{int} can be estimated by adding up the van der Waals forces between each graphene carbon atom and the substrate portion within a cut-off distance from this carbon atom. If the cut-off distance is large enough, such an estimate of interaction energy converges to the theoretical value of E_{int}. In all simulations reported in this paper, a cut-off distance of 3 nm was used and shown to lead to variations in the estimated value of E_{int} less than 1%.

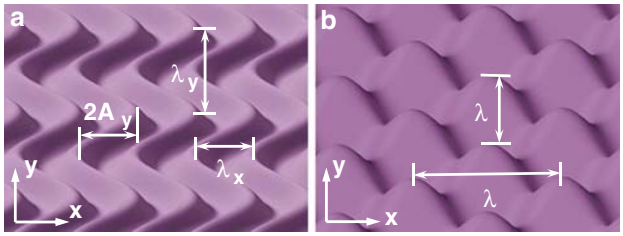

Fig. 1 Schematics of substrate surface corrugations: **a** herringbone and **b** checkerboard

We have developed a Monte Carlo numerical scheme to compute the multiple integrals in Eq. 1, as summarized below [25]. For the ith graphene carbon atom, n random locations are generated in the substrate portion within the cut-off distance from this carbon atom. The interaction energy between this carbon atom and the substrate is estimated by

$$E_i = (\rho_{\mathrm{s}}V_{\mathrm{s}}/n)\sum_{j=1}^{n} V_{\mathrm{LJ}}(r_{ij}), \tag{2}$$

where r_{ij} is the distance between the ith graphene carbon atom and the jth random substrate location. Equation 2 is evaluated at m equally spaced locations over the graphene of area S. The graphene–substrate interaction energy over this area can then be estimated by

$$E_{\mathrm{int}} = (\rho_{\mathrm{c}}S/m)\sum_{i=1}^{m} E_i. \tag{3}$$

As n and m become large enough, Eq. 3 converges to the theoretical value of E_{int}. In all simulations in this paper, $n = 10^6$, $m = 400$.

The strain energy in the graphene–substrate system results from the corrugating deformation of the graphene and the interaction-induced deformation of the substrate. When an ultrathin monolayer graphene partially conforms to a rigid substrate (e.g., SiO_2), the substrate deformation due to the weak graphene–substrate interaction is expected to be negligible. Also, when the graphene spontaneously follows the substrate surface under weak interaction (imagine a fabric naturally conforming to a rough surface) and is not subject to any mechanical constraints (e.g., pinning [26]), the in-plane stretching of the graphene is also expected to be negligible. Under the above assumptions, the strain energy in the graphene–substrate system can be reasonably estimated by the graphene strain energy due to out-of-plane bending, denoted by E_{g}. Effect of the above assumptions on results is to be further elaborated later in this paper. Denoting the out-of-plane displacement of the graphene by $w_{\mathrm{g}}(x, y)$, the graphene strain energy over an area S can be given by

$$E_{\mathrm{g}} = \int_S D\left(\frac{1}{2}\left(\frac{\partial^2 w_{\mathrm{g}}}{\partial x^2} + \frac{\partial^2 w_{\mathrm{g}}}{\partial y^2}\right)^2 - (1-\nu)\left(\frac{\partial^2 w_{\mathrm{g}}}{\partial x^2}\frac{\partial^2 w_{\mathrm{g}}}{\partial y^2} - \left(\frac{\partial^2 w_{\mathrm{g}}}{\partial x \partial y}\right)^2\right)\right)\mathrm{d}S, \tag{4}$$

where D and ν are the bending rigidity and the Poisson's ratio of graphene, respectively.

The out-of-plane herringbone corrugations of the substrate surface (Fig. 1a) and the out-of-plane corrugations of the graphene regulated by such a substrate surface are described by

$$\begin{aligned} w_s &= A_s \cos\big((2\pi/\lambda_x)(x + A_y \cos(2\pi y/\lambda_y))\big) - h \\ w_g &= A_g \cos\big((2\pi/\lambda_x)(x + A_y \cos(2\pi y/\lambda_y))\big), \end{aligned} \tag{5}$$

respectively, where A_s and A_g are the amplitudes of the substrate surface corrugations and the graphene corrugations, respectively; for both the graphene and the substrate, λ_x is the wavelength of the out-of-plane corrugations, λ_y and A_y are the wavelength and the amplitude of in-plane jogs, respectively; and h is the distance between the middle planes of the graphene and the substrate surface. Given the symmetry of the herringbone pattern, we only need to consider a graphene segment over an area of $\lambda_x/2$ by $\lambda_y/2$, and its interaction with the substrate. By substituting Eq. 5 into Eq. 4, the strain energy of such a graphene segment is given by

$$E_g = D\pi^4 A_g^2 \left(6\pi^4 A_y^4 + \lambda_y^4 + 2\pi^2 A_y^2 \left(\lambda_x^2 + 2\lambda_y^2\right)\right)/\lambda_x^3 \lambda_y^3. \tag{6}$$

As shown in Eq. 6, for a given substrate surface corrugation (i.e., A_s, A_y, λ_x, and λ_y), E_g increases monotonically as A_g increases. On the other hand, the graphene–substrate interaction energy, E_{int}, minimizes at finite values of A_g and h, due to the nature of van der Waals interaction. As a result, there exists a minimum of $(E_g + E_{int})$ where A_g and h reach their equilibrium values. The energy minimization was carried out by running a customized code on a high performance computation cluster. In all computations, $D = 1.41$ eV, $l = 0.142$ nm, $\rho_s = 2.20 \times 10^{28}/\text{m}^3$, $\sigma = 0.353$ nm and $A_s = 0.5$ nm, which are representative of a graphene-on-SiO_2 structure [27, 28]. Various values of ε, λ_x, λ_y, and A_y were used to study the effects of interfacial bonding energy and substrate surface roughness on the regulated graphene morphology.

Results and Discussion

Figure 2a plots the normalized amplitude of the regulated graphene corrugation, A_g/A_s, as a function of D/ε for various λ_x. Here $\lambda_y = 2\lambda_x$ and $A_y = \lambda_y/4$. Thus, various λ_x define a family of substrate surfaces with self-similar in-plane herringbone patterns and the same out-of-plane amplitude (i.e., A_s). For a given substrate surface pattern, if the interfacial bonding energy is strong (i.e., small D/ε), A_g tends to A_s. In other words, the graphene closely follows the substrate surface (Fig. 2b). In contrast, if the interfacial bonding is weak (i.e., large D/ε), A_g approaches zero. That is, the graphene is nearly flat and does not conform to the substrate surface (Fig. 2c). Interestingly, there exists a threshold value of D/ε, below and above which a sharp transition occurs between the above two distinct states of the graphene morphology. We call such a sharp transition *the snap-through instability of graphene*. The threshold value of D/ε increases as λ_x increases. For a given interfacial bonding energy, A_g increases as λ_x increases. That is, graphene tends to conform more to a substrate surface with smaller out-of-plane waviness.

Figure 3 shows the effect of in-plane waviness of the substrate surface on graphene morphology. Figure 3a plots A_g/A_s as a function of D/ε for various λ_y. Here $\lambda_x = 6$ nm and $A_y = \lambda_y/4$. For a given substrate surface pattern, if the interfacial bonding energy is strong (i.e., small D/ε), A_g tends to A_s. For a given interfacial bonding energy, A_g increases as λ_y/λ_x increases. That is, graphene tends to conform more to a substrate surface with smaller in-plane waviness. In particular, when λ_y/λ_x is large (e.g., 100), the predicted graphene corrugation amplitude converges to that of graphene regulated by straight substrate surface grooves with the same λ_x and A_s [25]. Figure 3b further plots A_g/A_s as a function of D/ε for various A_y with fixed λ_x and λ_y. Similar effect of in-plane waviness of the substrate surface on graphene morphology emerges from Fig. 3b. Moreover, the snap-through instability of graphene, similar to that illustrated in Fig. 2, is also evident in the results shown in Fig. 3.

The snap-through instability of graphene on a substrate surface can be explained as follows. Figure 4 plots the normalized total system energy as a function of A_g/A_s for various D/ε. Here $\lambda_x = 9$ nm, $\lambda_y = 2\lambda_x$ and $A_y = \lambda_y/4$. If the interfacial bonding energy is weaker ($D/\varepsilon = 575$) than a threshold value, the total energy profile reaches its minimum at a small graphene corrugation amplitude $A_g/A_s = 0.14$. If the interfacial bonding energy ($D/\varepsilon = 750$) is stronger than the threshold value, the total energy profile reaches its minimum at a large graphene corrugation amplitude $A_g/A_s = 0.93$. At the threshold value of $D/\varepsilon = 650$, the total energy profile assumes a double-well shape, whose two minima ($A_g/A_s = 0.20$ and 0.91) correspond to the two distinct states of the graphene morphology on the substrate surface.

In the case of graphene regulated by a substrate surface with checkerboard pattern (Fig. 1b), the substrate surface corrugations and the regulated graphene corrugations are described by

$$\begin{aligned} w_s &= A_s \cos(2\pi x/\lambda)\cos(2\pi y/\lambda) - h \\ w_g &= A_g \cos(2\pi x/\lambda)\cos(2\pi y/\lambda), \end{aligned} \tag{7}$$

respectively, where λ is the wavelength of the out-of-plane corrugations for both the graphene and the substrate

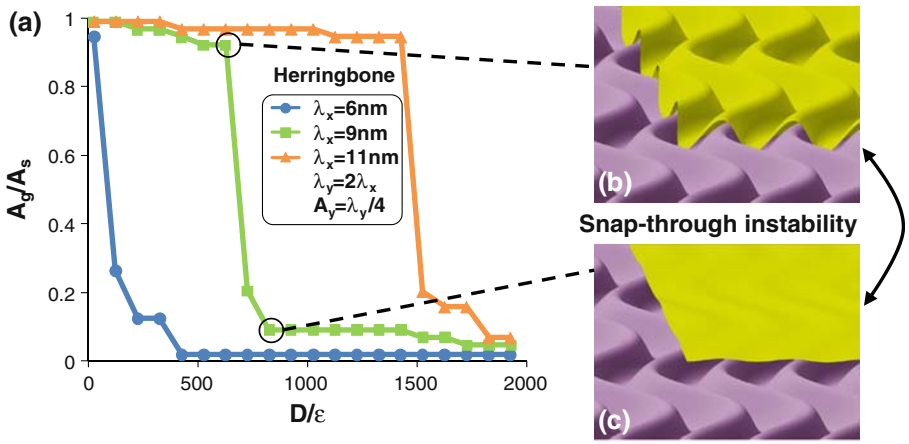

Fig. 2 **a** A_g/A_s on substrates with herringbone surface corrugations as a function of D/ε for various λ_x. At a threshold value of D/ε, the graphene morphology snaps between two distinct states: **b** closely conforming to the substrate surface and **c** remaining nearly flat on the substrate surface

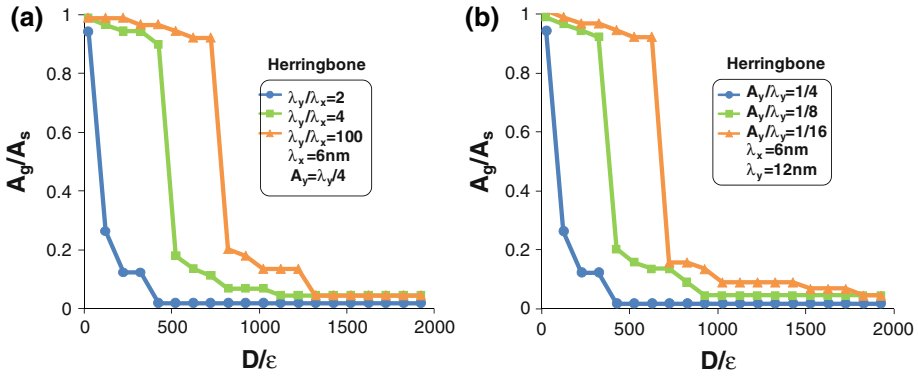

Fig. 3 Effects of in-plane waviness of the substrate surface on graphene morphology. **a** A_g/A_s as a function of D/ε for various λ_y. **b** A_g/A_s as a function of D/ε for various A_y. The snap-through instability of graphene morphology, similar to that shown in Fig. 2, is evident in both cases

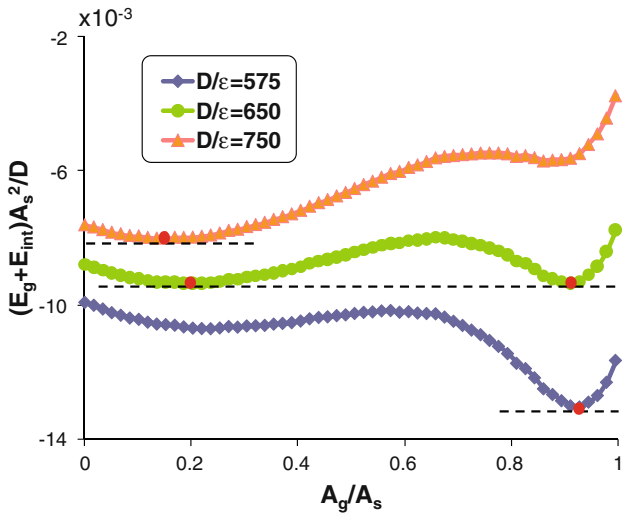

Fig. 4 The normalized total system energy as a function of A_g/A_s for various D/ε. At a threshold value of $D/\varepsilon = 650$, the total system energy minimizes at two points, corresponding to the two distinct states of graphene morphology. Here $\lambda_x = 9$ nm, $\lambda_y = 2\lambda_x$ and $A_y = \lambda_y/4$

surface. The numerical strategy similar to that aforementioned was implemented to determine the equilibrium amplitude of the regulated graphene morphology.

Figure 5 plots A_g/A_s regulated by the checkerboard substrate surface as a function of D/ε for various λ. For a given substrate surface roughness, A_g/A_s decreases as D/ε increases. For a given interfacial bonding energy, A_g/A_s increases as λ increases. On a substrate surface with checkerboard corrugations, graphene exhibits the snap-through instability as well, which also results from the double-well shape of the system energy profile at the threshold value of D/ε, similar to that shown in Fig. 4. The threshold value of D/ε at the graphene snap-through instability increases as λ increases.

In this paper we focus on graphene morphology spontaneously regulated by substrate surfaces via weak

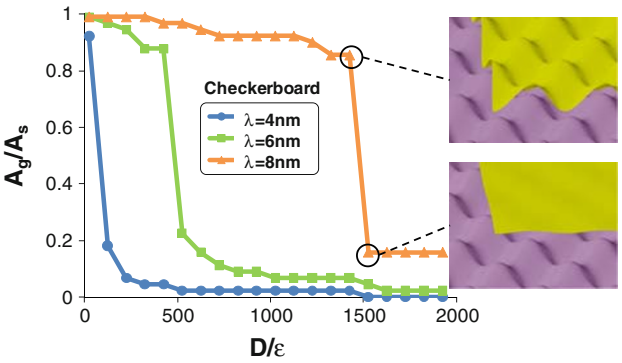

Fig. 5 A_g/A_s on substrates with checkerboard surface corrugations as a function of D/ε for various λ. The insets illustrate the two distinct states of graphene morphology at the snap-through instability

interaction. When a graphene/substrate structure is subject to external loading, the graphene strain energy due to stretching and the substrate strain energy may also need to be considered. In this sense, the present model overestimates the graphene corrugation amplitude. Also the graphene/substrate interaction can be enhanced by the possible chemical bondings or pinnings at the interface [26, 29, 30]. In this sense, the present model underestimates the graphene corrugation amplitude.

Concluding Remarks

In summary, we investigate the graphene morphology regulated by substrates with herringbone and checkerboard surface corrugations. Depending on interfacial bonding energy and substrate surface roughness, the graphene morphology exhibits a sharp transition between two distinct states: (1) closely conforming to the substrate surface and (2) remaining nearly flat on the substrate surface. The quantitative results suggest a promising strategy to control the graphene morphology through substrate regulation. While it is difficult to directly manipulate freestanding graphene [31], it is feasible to pattern the substrate surface via lithography [21, 22] and strain engineering [23, 24]. The regulated graphene morphology on such engineered substrate surfaces may lead to new pathways to control the graphene electronic properties, introducing desirable properties such as band-gap, or p/n junction behavior. In particular, the results shown in this paper (e.g., Figs. 2, 3, 5) reveal a wide range of design tunability of the graphene snap-through instability on substrates through substrate surface patterning and interfacial adhesion tailoring, which offers abundant unexplored potential toward the design of functional graphene device components (e.g., nano-switches, nano-resonators). We then call for experimental demonstration of these envisioned concepts.

Acknowledgment This work is supported by the Minta-Martin Foundation, a UMD General Research Board summer research award to T. L., and NSF CMMI 0856540. Z.Z. also thanks the support of the A. J. Clark Fellowship.

References

1. K.S. Novoselov, A.K. Geim, S.V. Morozov, D. Jiang, Y. Zhang, S.V. Dubonos, I.V. Grigorieva, A.A. Firsov, Science **306**, 666 (2004)
2. A.K. Geim, K.S. Novoselov, Nat. Mater. **6**, 183 (2007)
3. K.S. Novoselov, D. Jiang, F. Schedin, T.J. Booth, V.V. Khotkevich, S.V. Morozov, A.K. Geim, Proc. Natl Acad. Sci. USA **102**, 10451 (2005)
4. M.I. Katsnelson, Mater. Today **10**, 20 (2007)
5. A.K. Geim, Science **324**, 1530 (2009)
6. X. Wang, L. Zhi, K. Mullen, Nano Lett. **8**, 323 (2008)
7. G. Eda, G. Fanchini, M. Chhowalla, Nat. Nanotechnol. **3**, 270 (2008)
8. F. Schedin, A.K. Geim, S.V. Morozov, E.W. Hill, P. Blake, M.I. Katsnelson, K.S. Novoselov, Nat. Mater. **6**, 652 (2007)
9. M.D. Stoller, S.J. Park, Y.W. Zhu, J.H. An, R.S. Ruoff, Nano Lett. **8**, 3498 (2008)
10. K.S. Kim, Y. Zhao, H. Jang, S.Y. Lee, J.M. Kim, J.H. Ahn, P. Kim, J.Y. Choi, B.H. Hong, Nature **457**, 706 (2009)
11. A. Fasolino, J.H. Los, M.I. Katsnelson, Nat. Mater. **6**, 858 (2007)
12. J.C. Meyer, A.K. Geim, M.I. Katsnelson, K.S. Novoselov, T.J. Booth, S. Roth, Nature **446**, 60 (2007)
13. S.V. Morozov, K.S. Novoselov, M.I. Katsnelson, F. Schedin, L.A. Ponomarenko, D. Jiang, A.K. Geim, Phys. Rev. Lett. **97**, 016801 (2006)
14. A.H.C. Neto, F. Guinea, N.M.R. Peres, K.S. Novoselov, A.K. Geim, Rev. Mod. Phys. **81**, 109 (2009)
15. M. Ishigami, J.H. Chen, W.G. Cullen, M.S. Fuhrer, E.D. Williams, Nano Lett. **7**, 1643 (2007)
16. E. Stolyarova, K.T. Rim, S. Ryu, J. Maultzsch, P. Kim, L.E. Brus, T.F. Heinz, M.S. Hybertsen, G.W. Flynn, Proc. Natl Acad. Sci. USA **104**, 9209 (2007)
17. U. Stoberl, U. Wurstbauer, W. Wegscheider, D. Weiss, J. Eroms, Appl. Phys. Lett. **93**, 051906 (2008)
18. F.V. Tikhonenko, D.W. Horsell, R.V. Gorbachev, A.K. Savchenko, Phys. Rev. Lett. **100**, 056802 (2008)
19. V. Geringer, M. Liebmann, T. Echtermeyer, S. Runte, M. Schmidt, R. Ruckamp, M.C. Lemme, M. Morgenstern, Phys. Rev. Lett. **102**, 4 (2009)
20. J.H. Chen, M. Ishigami, C. Jang, D.R. Hines, M.S. Fuhrer, E.D. Williams, Adv. Mater. **19**, 3623 (2007)
21. Y. Xia, J.A. Rogers, K.E. Paul, G.M. Whitesides, Chem. Rev. **99**, 1823 (1999)
22. S.Y. Chou, P.R. Krauss, P.J. Renstrom, Science **272**, 85 (1996)
23. W.M. Choi, J. Song, D.-Y. Khang, H. Jiang, Y.Y. Huang, J.A. Rogers, Nano Lett. **7**, 1655 (2007)
24. X. Chen, J.W. Hutchinson, J. Appl. Mech. **71**, 597 (2004)
25. T. Li, Z. Zhang, submitted, Preprint: http://arxiv.org/abs/0907.1639 (2009)
26. P.J. Feibelman, Phys. Rev. B **77**, 165419 (2008)
27. D. Tománek, W. Zhong, E. Krastev, Phys. Rev. B **48**, 15461 (1993)
28. J.N. Israelachvili, *Intermolecular and Surface Forces* (Academic Press, London; San Diego, 1991)
29. S. Namilae, N. Chandra, J. Eng. Mater. Technol. Trans. ASME **127**, 222 (2005)
30. J. Sabio, C. Seoanez, S. Fratini, F. Guinea, A.H.C. Neto, F. Sols, Phys. Rev. B **77**, 195409 (2008)
31. L. Tapaszto, G. Dobrik, P. Lambin, L.P. Biro, Nat. Nanotechnol. **3**, 397 (2008)